

Local Temperature Profile Measurement in Microchannels Using Temperature Sensitive Leuco-Dye Microbeads

Marco A. Cartas-Ayala and Rohit Karnik*

Department of Mechanical Engineering, Massachusetts Institute of Technology,
77 Massachusetts Ave., Cambridge, Ma 02139 USA

ABSTRACT

Microfluidics has shown the ability to reproduce many of the techniques used in chemistry and biology, achieving faster and inexpensive results with smaller samples. As part of this effort towards miniaturization, the heating and cooling of samples has become an important step in many devices, especially for nucleic acid analysis. Measuring temperature profiles inside microchannels is required to verify the performance of such devices. Here we introduce a new technique to measure thermal profiles in microchannels: leuco-dye temperature sensitive microbeads, which permits fast, simple and inexpensive measurement of thermal profiles based on color, which enable its use to quickly assess temperature profiles to verify device performance, or as an educational tool for visualizing microscale heat transfer. Using the technique, we present visualization of thermal profiles and measurement of color transition lengths in microfluidic devices and compare the results with theoretical and numerical models with good agreement.

Keywords: Thermal profile, temperature measurement, microfluidics, microbeads, heat transfer, cooling, microreactors, polymerase chain reaction (PCR)

NOMENCLATURE

Cp_f	Specific heat capacity of the fluid [J/kgK]
D	Hydraulic diameter [m]
k_m	Thermal conductivity of material m , where $m = f$ (fluid), g (glass), p (PDMS) [W/mK]
L	Channel length [m]
\dot{m}	Mass flow rate [kg/s]
Nu_D	Nusselt number based on the hydraulic diameter
p	Pressure [N/m^2]
Re_D	Reynolds number based on the hydraulic diameter
T	Temperature [$^{\circ}C$]
T_{∞}	Ambient temperature [$^{\circ}C$]
u	Streamwise velocity [m/s]
u_m	Average velocity [m/s]
V_{avg}	Average Velocity [m/s]
x	Stream wise co-ordinate [m]
x_e	Thermal entry length [m]
ΔP	Pressure Drop [N/m^2]
∇^2	Laplacian [$1/m^2$]
ρ_m	Density of the material m , where $m = f$ (fluid), g (glass), p (PDMS)
μ	Dynamic viscosity [kg/ms]

*Corresponding author. karnik@mit.edu, Tel: (617) 324-1155.

1. INTRODUCTION

1.1. Heat transfer in microsystems

Microfluidics, the manipulation and control of liquids in channels with sub-millimeter dimensions, has been used since the early nineties to improve conventional chemical, biological and physical assays. By using reduced volume geometries, microfluidics offers several advantages over macro scale assays: reduced sample volume [1, 2], faster cooling and heating of samples [3, 4], portability [5, 6], disposability [7, 8] and integration of multiple complex assays in a reduced volume. Microfluidics also finds applications in nano and micro particle fabrication [9, 10], DNA amplification [11], proteomics [12], electronics cooling [13], and microturbines for energy generation [14].

As the research in microfluidics expands, it is increasingly common to include heating and cooling steps in the microfluidic devices. A clear example of such trend is DNA sequencing, which has evolved from simple sample detection using microfluidic channels to complete sample handling: from sample purification and DNA amplification by polymerase chain reaction (PCR) to separation and sequencing within the same device [15]. In fully integrated DNA sequencing, cooling and heating is required for DNA amplification, i.e. to generate more copies of the same DNA sequence. Since the chemical kinetics of DNA amplification are thermally driven, adequate cooling and heating is critical for proper DNA amplification; if temperatures are too low or too high, the PCR reaction steps fail. Further, microscale heat-transfer is important not only for biological assays; for instance, cold liquid flowing through microfluidic channels has been used to cool microprocessors [13] and properly regulating the temperature of microreactors can maximize their efficiency [14].

As heating and cooling becomes widely used in microsystems, several new problems emerge due to the reduced dimensions used. For instance, in PCR amplification of DNA, sample needs to be heated and cooled repeatedly, and cold and hot zones need to be designed as close as possible to minimize heating time, resulting in sharper thermal profiles. Since the thermal profiles and the rates of heat transfer scale as $\Delta T/L$, maintaining sharp temperatures changes over smaller dimensions increases undesired parasitic heat flows. As a result, important space within devices might need to be sacrificed in order to minimize temperature perturbations that can modify the efficiency of the target reaction. Additionally, designing and simulating devices within a microenvironment imposes additional restrictions not normally encountered in macroscale reactor design, e.g. the fluid domain and solid domain containing the channels are thermally fully coupled by thermal diffusion and convection, and conjugate heat transfer is necessary to adequately describe the problem. Further, even if adequate thermal design is performed and thermal diffusion is minimized or accounted for, e.g. using numerical simulations, verification of the designed temperature as a function of position, thermal profile, is indispensable to ensure proper function of miniaturized devices. For such purposes the thermal profile must be measured directly.

Additionally, a reaction performed successfully in a macro environment might present extra challenges particular to the micro environment: large surface to volume ratios which cause large evaporation areas, unusually large surface interaction of the walls with the chemical reaction, large diffusion-limited mixing times and possible channel blockage due to solid byproducts. These problems require considerable time and effort to fix or even diagnose. Thus, for troubleshooting of failed PCR reactions, for example, verifying the thermal profile should be the first step, before exploring the effects of surface passivation and chemistry that can require considerable efforts.

1.2. Techniques used to measure thermal profiles in microfluidic devices

Four techniques have been used to measure thermal profiles inside micro channels: thermal cameras [16], micro fabricated temperature sensors (temperature sensitive resistors) [17], temperature sensitive fluorescent dyes [18] and temperature sensitive crystals [19].

Thermal cameras have several limitations when used to measure temperature profiles in micro reactors. First, thermal cameras are expensive and for the same reason commonly unavailable. Second, calibration of the thermal emissivity of each material used in the micro device is needed for measurement to be valid, which makes temperature measurement complex when multiple materials are used. Third, a thermal camera only captures the thermal profile of material close to the surface; as a result, when thick devices are manufactured, a thermal camera is incapable of providing information of the bulk of the material where the channels are located.

Micro fabricated thermal sensitive resistors have been used when the incorporation of temperature sensitive resistors is possible. The microfabricated resistors provide an accurate way to measure temperature locally, but the extra fabrication step is not possible for many devices and the fabrication of microelectrodes results in extra costs and increased complexity during fabrication.

Using thermal-sensitive fluorescent dyes is an inexpensive and easier alternative to the use of resistors, but since different channel thickness and widths produce a different fluorescent intensity, this method requires re-calibration of the camera for every geometry used, furthermore, since many of the fluorescent dyes rapidly diffuse into the polymers used to fabricate micro channels, e.g. Rhodamine B into polydimethylsiloxane, the calibration factor changes with time, producing uncertainty in the measured temperatures as time progresses.

Transient liquid crystals, structured solids that become temporarily liquid while temperature is kept above a crystal-specific temperature, have been used to measure temperature profiles in PCR devices [18]. As crystals are heated, they experience a phase change that is accompanied by a color change. The use of transient liquid crystals improves on many of the deficiencies of the previous methods; it is less expensive than using thermal cameras, and easier to use than the thermal sensitive fluorescent dyes (diffusion is not observed and signal does not change with time.) Nevertheless, liquid crystals still have drawbacks. Phase transition occurs at a given fixed temperature, which limits the application of the crystals to a single temperature. Further, the phase transition change requires a non-negligible amount of energy that delays the thermometric response time, which limits their application to non-dynamic environments, i.e. slow microfluidic flows.

Here, we present a new technique based on the use of leuco-dye thermally sensitive micro beads (TuBeads) to measure the local temperature profile. This technique has the following advantages: it is inexpensive and easy to use, permits the measurement of the temperature profile locally, and since micro beads do not diffuse into the channel material it is insensitive to time as the experiment progresses. Furthermore, since it is often more convenient to measure the temperature surrounding the microchannel rather than the fluid temperature itself (and vice-versa), two variations of the technique were explored: TuBeads embedded in the PDMS walls, and TuBeads in solution to measure in situ temperature profiles. The presence of TuBeads embedded in the channel walls is a new approach that enables the use of a larger variety of liquids not compatible with the beads.

1.3. Leuco-dye beads

Leuco-dye beads used in this paper are the main component of thermal sensitive paints. Thermal sensitive paints have multiple commercial applications, from decorative purposes to thermal indicators. As thermal indicators they have been used in a wide range of applications, from food and beverages to alkaline-batteries charge indicators. Leuco dyes are chemicals that have two molecular configurations: leuco (colorless) and colored, which can be switched by the application of UV light or heat [19]. Different leuco molecules can be switched at different temperatures; there are commercially available leuco dyes with color transition temperatures between -6 and 60°C . Color change of leuco dyes is not a step function, color changes gradually in an interval of $\sim 4^{\circ}\text{C}$. When leuco dyes are encapsulated the particles generated are normally not uniform, the particles have a wide distribution, ranging in size between 3 to 15 microns, as shown in Figure 1.

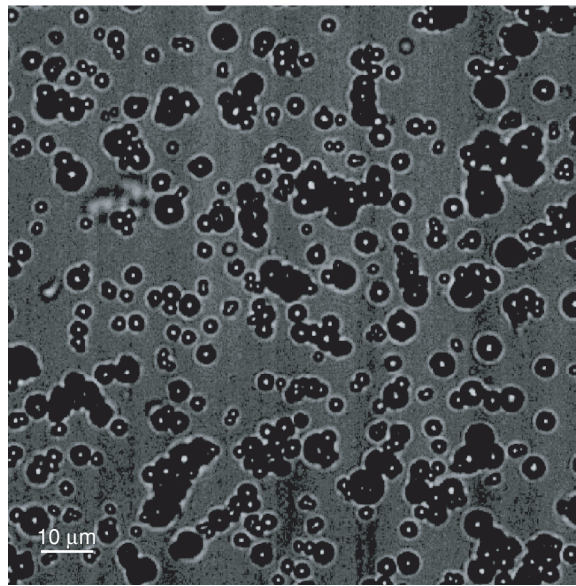


Figure 1. Micrograph of the temperature sensitive beads.

2. MATERIALS AND METHODS

2.1. Temperature sensitive beads

Temperature sensitive beads, Indigo-Blue-to-Clear, were purchased from Thermochemicals (Denver, CO). Indigo-Blue-to-Clear beads change color at 30°C (different transition temperature beads are also available, blue was selected for its high contrast). Temperature sensitive beads were mixed with water to form a solution of 10 mg/mL. Following the initial mix, the solution was filtered using filtering tissue, which prevented the formation of particle-agglutinations in the mix.

2.2. Characterization of the thermal sensitive beads

Characterization of the temperature sensitive micro-beads is essential before measurement of any thermal profile. Two properties are relevant to properly measure a thermally dynamic system: response time and color transition temperature spread.

Response Time. The time required to warm/cool down the beads establishes the response time. Thermal beads are polymer microspheres of diameter less than 10 μm (average size is approximately 6 μm from microscope images, Figure 1). The characteristic time needed to change temperature of the particle, τ , scales as $\tau \sim R^2/\alpha$, where R is the particle radius and α is the thermal diffusivity. The thermal properties of the microspheres are not specified by the manufacturer, but from a survey of common polymers for encapsulation, we can estimate the characteristic time. Assuming α ranges from 10^{-7} to 10^{-8} m^2/s typical for polymers, τ ranges from 0.25 to 2.5 ms. Then, particle color will reflect not only the temperature of the place the particle occupies at the current time, but the averaged temperature of the places it had been in the last 2.5 milliseconds, or a traveled distance $x = u\tau$, where u is the flow velocity. It follows that in order to have a reliable temperature measurement within 50 μm (a typical channel height), the maximum allowed velocity is 5 cm/s, a value larger than velocities normally achieved in most microfluidic devices. Then, response time does not limit the applicability of microbeads to measure thermal profiles in microfluidic devices.

Color Transition Temperature. Once response time was estimated, we characterized the particle's color transition. For that purpose, 100 mL of the microbead solution prepared as mentioned before was warmed up to temperatures between 26 and 35°C and color change was characterized using a digital camera. The solution was stirred between measurements to achieve temperature uniformity. In addition,

constant illumination conditions were achieved by replacing natural light with white lamps in a darkened room. Briefly, for the setup we measured reflected light coming from 1 cm depth of the bead solution in a glass container heated from the bottom by a white ceramic hot plate. The camera, an Exilim EX-H25, was located 10 cm from the water surface. Light was shone from the side forming an angle of roughly 15° from the surface.

Experimentally it was determined that the transition temperature occurs within $\pm 3.3^\circ\text{C}$ of the specified transition temperature, 30°C . The beads started to change color at 27.8°C and at 33.3°C the beads had transitioned completely. Then, based on color change, we can accurately measure temperatures within the interval of 26.6°C and 33.3°C , as shown in Figure 2. Further analysis can be done per color using the average normalized intensity information shown in Figure 2. The red channel intensity at temperatures below temperature transition is approximately zero and changes to an intensity level of roughly a 100. The green channel intensity also increases, but only from 110 to 150, a smaller amount than the red line. The blue channel intensity decreases from roughly 210 to 150. Since the red signal experiences the largest increment, it can be used as main criterion for temperature transition. Alternatively, a combination of the three intensity signals can be used to get a larger intensity signal and minimize noise. The intensity change in the three channels is a non-linear function of temperature, fact that should be considered if high temperature resolution is necessary. Compensation using a look up table of function curve fitting is possible but not implemented in this work. It must be noted that if this method is used, illumination conditions must be kept as constant as possible since changes in illumination change the base level and will cause noise in the measurement, which can be observed in some of the frames in the calibration chart. Particularly, in the last measurement for the green light a decrement in the green light intensity is observed, but it can be attributed to a small intensity decrement in the illumination conditions since the other two colors also suffered an intensity change.

2.3. Microchannels

The micro fabricated devices used for the experiments were 12-turns zigzag channels. Each channel had a rectangular cross section of $800\ \mu\text{m}$ width with $150\ \mu\text{m}$ height, as shown in Figure 3.

Standard lithography was used to fabricate the molds. Briefly, a silicon wafer was spin coated with SU-8 photoresist to achieve a $150\ \mu\text{m}$ photoresist layer. Then, the photoresist was developed. Finally, the mold was silanized to avoid PDMS adhesion by placing the wafer in a large covered Petri dish containing several drops of perfluorooctyltrichlorosilane (Sigma Aldrich) for 10 min.

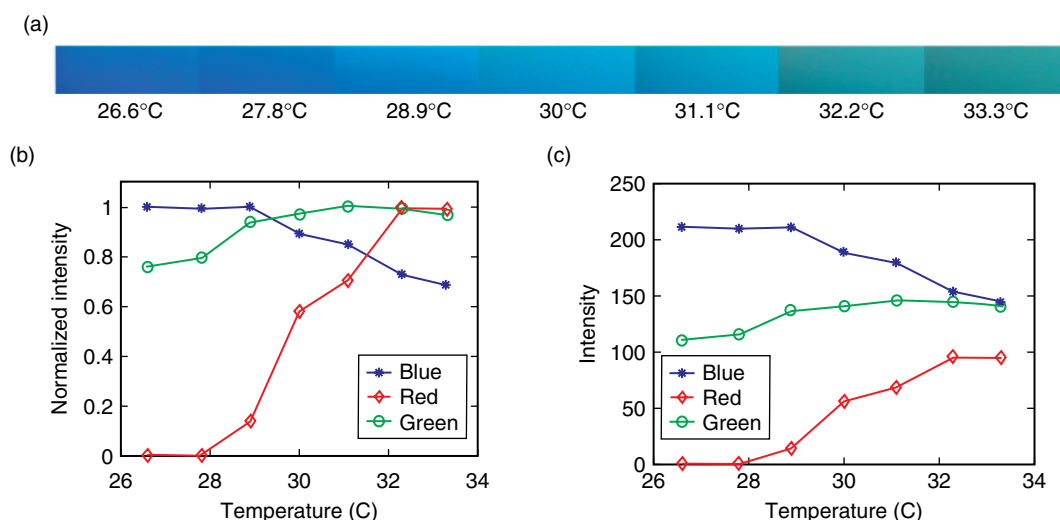


Figure 2. (a) Color of TuBeads at different temperatures. (b) Color response normalized by maximum intensity for each color. (c) Color response without normalization.

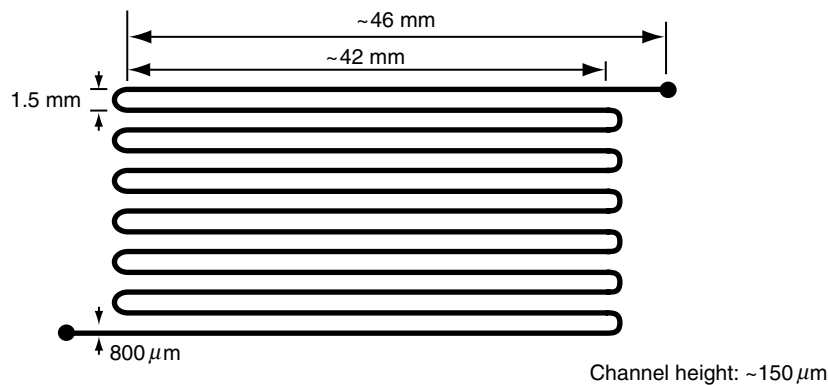


Figure 3. Microchannel devices.

Two kinds of devices were used in experiments: PDMS only devices and TuBeads embedded devices. Both devices were fabricated using Sylgard 184 (Dow Corning) using variations of the soft lithography method. In both cases, designed channel geometries differed from the fabricated ones by less than $10\ \mu\text{m}$ due to fabrication inaccuracies, roughly 3% with respect to the channel height.

PDMS-only devices were fabricated by soft lithography. The devices consisted of two parts: upper part, which contained the molded channels, and bottom part, which sealed the channels. Briefly, PDMS-only channels were fabricated as follows. PDMS 184 from Dow Corning was mixed using a 10:1 ratio by weight. To fabricate the upper part, PDMS was poured into the mold forming a 4 mm layer. Next, the PDMS was degassed and baked at 80°C for 30 min. Then, the PDMS mold containing the micro channels was cut using a clean razor blade, perforated to form the channel inlets using a biopsy punch ($0.5\ \text{mm}$ internal diameter punch from Harris Uni-Core), and cleaned using isopropanol. The bottom layer that sealed the channels was fabricated as follows. 10:1 PDMS was spin coated on top of a blank silicon wafer forming a $150\ \mu\text{m}$ PDMS layer. Then, the blank wafer coated with PDMS was baked for 30 min at 80°C . Finally, the PDMS channels and sealing layer were bonded using air plasma for 30 s at 500 mTorr (Expanded Plasma Cleaner, Harrick Plasma, Ithaca, NY).

TuBeads embedded devices were fabricated to have a $500\ \mu\text{m}$ TuBeads/PDMS layer, where the channels are embedded, and a 3.5 mm PDMS-only layer that provided structural rigidity. The TuBeads devices use the same mold as the PDMS-only devices. TuBeads embedded PDMS were fabricated as follows. PDMS 184 from Dow Corning was mixed using a 10:1 ratio. Then, using a Thinky mixer for 60 s at 1000 RPM (Thinky USA, Laguna Hills, CA), 0.1 g/mL of TuBeads were incorporated into the

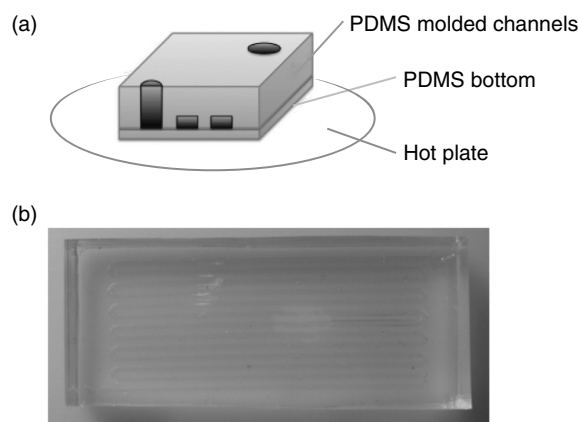


Figure 4. PDMS-only devices. (a) Schematic. (b) Photograph.

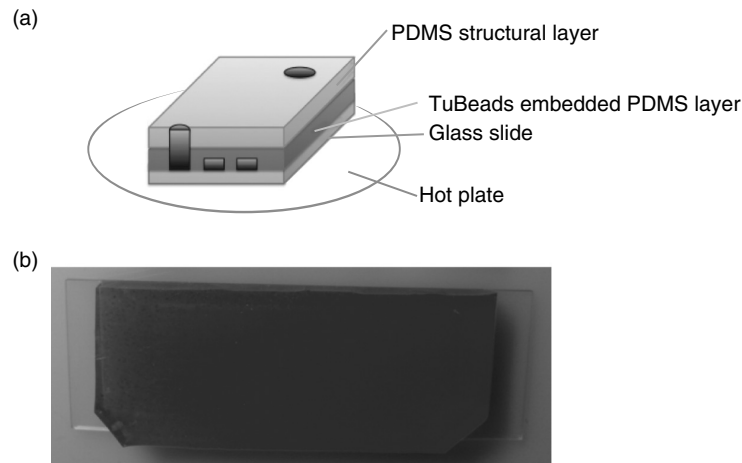


Figure 5. TuBEads embedded PDMS devices. (a) Schematic. (b) Photograph.

PDMS mix. A 500 μm TuBeads/PDMS layer was spin coated on the microchannel mold. Next, PDMS was degassed and baked at 50°C overnight. Then, a second layer 3.5 mm thick PDMS layer was added to the mold to provide rigidity, again baking at 50°C overnight. Next, the PDMS molded piece was cut using a clean razor blade, perforated using a biopsy punch (0.5 mm internal diameter punch from Harris Uni-Core) to form the channel inlets, and cleaned using isopropanol. Finally, PDMS channels and glass slides were bonded using air plasma as described before.

2.4. Thermal profile measurement

2.4.1. PDMS only devices

First, to demonstrate the capability of the TuBeads technique to determine flow temperature profiles within the fluid domain, the TuBeads solution was flown through the PDMS-only devices. Thermal and flow conditions used are as follows. The bottom of the PDMS-only device was subjected to a constant temperature of 35°C by placing it on top of a ceramic-top temperature regulated hot plate. The temperature of the hot plate was additionally verified by using a thermocouple adhered to the surface placed next to the device. The TuBeads mix was flown from a reservoir kept at room temperature (14°C) and regulated pressure. Pressure in the reservoir was changed from 1800 Pa to 9000 Pa every 1800 Pa in order to achieve different flow velocities.

After each flow condition was imposed, 20 minutes were allowed between measurements to achieve thermal equilibrium. Images were taken using an Exilim EX-H25 camera keeping illumination

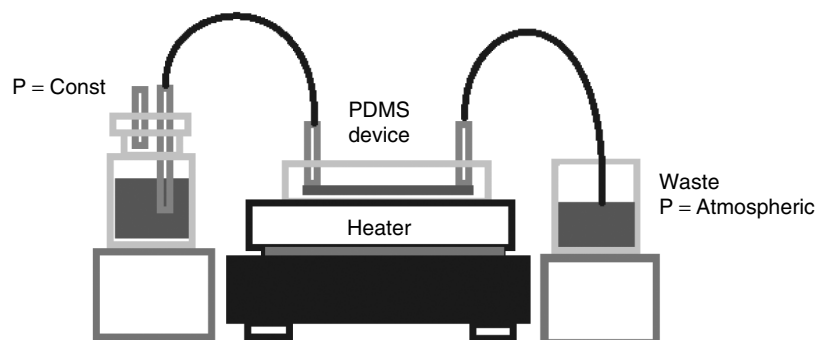


Figure 6. Schematic of the experimental setup.

conditions constant. Additionally, the output liquid was collected over 5 minutes to measure flow rates inside the devices.

2.4.2. TuBeads embedded devices

Second, in order to demonstrate the capacity of the TuBeads technique to determine temperature profiles within the solid domain, deionized water was flown through the TuBeads-embedded PDMS devices. Thermal and flow conditions used are as follows. The bottom of the device was subjected to a constant temperature of 35°C by placing it on top of a ceramic-top temperature-regulated hot plate. The temperature of the hot plate was additionally verified by using a thermocouple adhered to the surface placed next to the device. Water was flown from a reservoir kept at 4°C and at regulated pressure of ~50 kPa. Again, images were taken using an Exilim EX-H25 camera keeping illumination conditions constant.

2.5. Numerical simulation

To compare the performance of the TuBeads technique, a 3D simulation of the PDMS and fluid domains was performed using Comsol Multiphysics 4.0. The numerical simulation solves within the fluid domain the heat transfer equation with convective terms

$$\frac{\rho_f C_p}{k_f} (\bar{u} \cdot \nabla T) = \nabla^2 T, \quad (1)$$

and within the solid domain

$$0 = \nabla^2 T. \quad (2)$$

At the same time, steady state Navier-Stokes equations were solved to determine the proper fluid velocities used in the heat transfer equation for the fluid domain. The solid domain thermal conductivity used was: k_p (PDMS) = 0.15 W/mK. For the fluid domain, water properties embedded in Comsol 4.0 were used, which allowed for temperature dependence to be included in the simulation. In this simulation, the thermal properties of the beads in the flown mix were neglected since they constituted ~1% of the total mass flowing inside the device at a given time. Inlet and environment temperatures were set to 14°C.

All dimensions were kept the same as in the designed devices: channel turns, length, width and thickness. The microchannels had a thickness of 150 μm while the PDMS layer was 4 mm, which suggest the use of different meshing schemes for each domain. For the fluid domain the option “boundary layer” meshing was used.

For the solid domain a coarse free-tetrahedral meshing scheme was used. The maximum element size was set to 7 mm, and the minimum to 30 μm . For the fluid domain, a three level boundary layer with a stretching factor set to two was used. Finally, the boundary conditions used are as follows. On the upper and lateral surfaces, upper-plate and vertical wall convective cooling boundary conditions were used. Comsol automatically updates the convective coefficient on these walls, as the surface temperature is determined through the iterations. On the bottom side of the domain, a constant temperature of 35°C was imposed.

The surface contact resistance was neglected since the roughness between the PDMS and plate was smaller than 1 μm . The PDMS roughness is similar to that of the silicon wafer from which it was molded, <100 nm, and that of the hot plate is smaller than 1 μm (which is necessary to create a reflective surface). Overall, this extra resistance can represent as much as an additional equivalent 10 μm thick layer of PDMS between the hot plate and the fluid, inducing a thickness variation of as much as 6% with respect to the designed device.

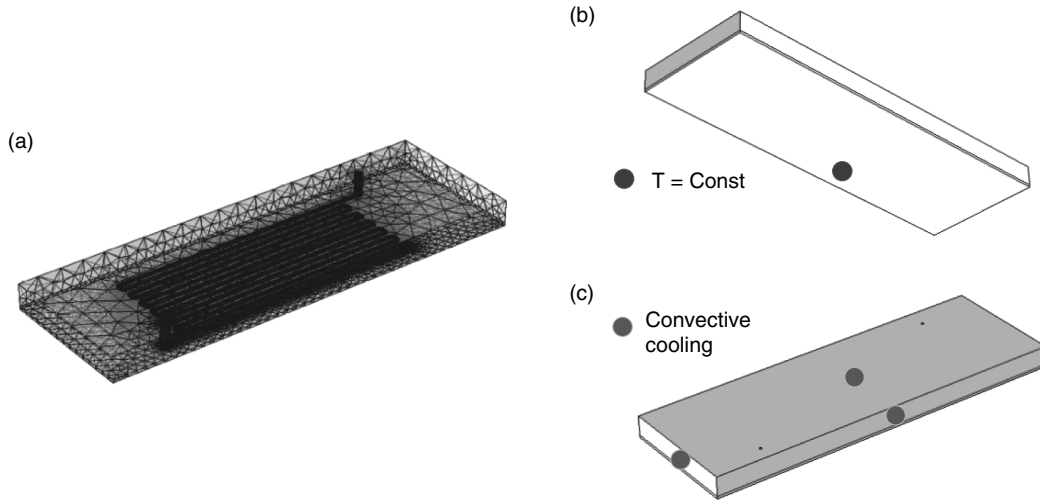


Figure 7. (a) Meshing used in Comsol Multiphysics 4.0. (b) View of the Bottom PDMS Surface. (c) Upper PDMS Surface. Bottom surface was kept at constant temperature, while convective boundary conditions were applied to all the other surfaces.

3. RESULTS AND DISCUSSION

3.1. PDMS only devices

In order to test the device performance we present a comparison of the theoretical, experimental and simulated thermal development lengths. First we discuss the design criteria and theoretical considerations involved in designing the channels.

The channels used in the experimental section were designed to create a wide range of velocities to test the ability of the TuBeads technique. For fully developed laminar flow and the designed rectangular cross section, pressure drop and velocity are related by Darcy's law [21],

$$\frac{77}{\text{Re}_D} = -\frac{dp}{dx} \frac{D}{\frac{1}{2}\rho u_m^2}, \quad (3)$$

where D is the hydraulic diameter, Re_D is the Reynolds number based on the hydraulic diameter, ρ the fluid density, u_m the average velocity and $\frac{dp}{dx}$ the pressure gradient. Using equation (3), assuming

uniform pressure drop per unit length, using 100 kPa at the channel entrance, a channel length of 0.6 m (typical length for a folded microchannel), water density of 1000 kg/m³ and viscosity of 0.001 kg/m-s, it was determined that for a velocity range of 0–0.1 m/s a hydraulic diameter in the order of 0.25 mm was required. For that purpose, the channel dimensions were set to be 150 μm height by 800 μm width. From the estimated velocity range, a Reynolds smaller than 25 was expected. Since the Reynolds number range is moderate, not high enough to produce turbulence but large enough for inertia to be an important or dominant factor over the target range, the flow is expected to be laminar but not fully viscous.

For laminar flow, the thermal entry length, x_e , is related to the Reynolds number, Re , and Prandtl number, Pr , by the following equation [21]

$$\frac{x_e}{D} \approx 0.05 \text{Re Pr} \quad (4)$$

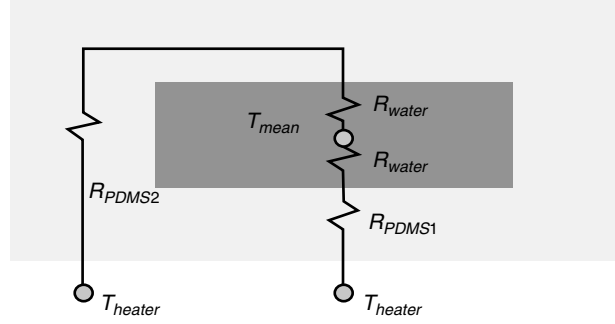


Figure 8. Resistance Model used to estimate the average channel surface.

Using a Prandtl number for water of 7.14, a hydraulic diameter of 0.25 mm, and a Reynolds number of 25, the thermal entrance length was calculated to be 2.2 mm. Then, since the velocity entry length is smaller than the thermal entry length because of the large Prandtl number ($Pr > 1$), the velocity and thermal profiles inside the micro channels can be assumed to be fully developed for most of the length of the channel. Further, for fluid flowing through a tube, from energy conservation, the following equation can be obtained [21],

$$\frac{dT_{mean}}{dx} = \frac{P}{\dot{m}c_{p,f}} h(T_{wall} - T_{mean}), \quad (5)$$

where T_{wall} is the channel wall temperature, T_{mean} is the mean temperature at a given position x along the channel, P is the channel perimeter, \dot{m} is the mass flow rate, $c_{p,f}$ is the specific heat capacity of the fluid and h is the heat transfer coefficient. Now, since the bottom of the device is set to a constant temperature through a regulated heat source, it is reasonable to assume as a first order approximation a constant temperature is imposed on the channel walls. Then, h can be estimated by using the Nusselt number, Nu_D , for constant temperature rectangular channels of aspect ratio 800/150, [21]

$$Nu_D = \frac{hD}{k} = 5, \quad (6)$$

where k is the thermal conductivity of water. Notice that since constant wall temperature value is just an approximation, the temperature difference between the fluid and the wall is an approximation too. In order to have a better estimate of how the PDMS bottom layer affects h , we used a one dimensional resistance model. There are two possible paths for heat transfer to occur from the PDMS bottom surface (which is at constant temperature T_{heater}) into the mid-plane of the channels. In the first path, heat travels through two resistances in series: a $160 \mu\text{m}$ PDMS layer and a $75 \mu\text{m}$ water layer, with thermal conductivities of 0.15 W/mK and 0.58 W/mK respectively. In the second path, heat transfer occurs through the bottom PDMS surface, around the channel and into the wall further away from the heating plate.

Then, the differential equation that governs the mean temperature of the fluid becomes

$$\frac{dT_{mean}}{dx} = \left(\frac{Px}{2\dot{m}Cp_f} \left[\frac{R_{water}}{R_{water} + R_{PDMS1}} + \frac{R_{water}}{R_{water} + R_{PDMS2}} \right] h \right) (T_{heater} - T_{mean}), \quad (7)$$

where R_{water} and R_{PDMS} are the equivalent thermal resistances of water and PDMS layers. Now, solving the differential equation for a fully developed thermal and fluid profile inside a tube with constant wall temperature, the mean temperature changes according to the equation

$$\frac{T_{heater} - T_{mean}(x)}{T_{heater} - T_{mean}(x=0)} = \exp\left(-\frac{Px}{2\dot{m}Cp_f} \left[\frac{R_{water}}{R_{water} + R_{PDMS1}} + \frac{R_{water}}{R_{water} + R_{PDMS2}} \right] h\right), \quad (8)$$

$$\frac{T_{heater} - T_{mean}(x)}{T_{heater} - T_{mean}(x=0)} = \exp\left(-\frac{Px}{\dot{m}Cp_f} \alpha h\right), \quad (9)$$

where

$$\alpha = \frac{1}{2} \left[\frac{R_{water}}{R_{water} + R_{PDMS1}} + \frac{R_{water}}{R_{water} + R_{PDMS2}} \right], \quad (10)$$

Then, the fluid will achieve a constant temperature according to

$$-\ln\left(\frac{T_{heater} - T_{mean}(x)}{T_{heater} - T_{mean}(x=0)}\right) \frac{1}{\alpha} \frac{ACp_f \rho_f}{Ph} u_{mean} = x, \quad (11)$$

where A is the channel area, ρ is the fluid density and u_{mean} is the average channel velocity. According to this equation, the position at which the dye color transition occurs should be directly proportional to the channel velocity. Now, from Darcy's equation,

$$u_{mean} = -\frac{2D^2}{77\mu L} \Delta P, \quad (12)$$

the average velocity, u_{mean} , is proportional to the pressure applied to the device, then the thermal development length should be directly proportional to the pressure. Since we are neglecting heat flow from the upper channel surface to the environment and we are assuming constant wall temperatures, the model is an approximation. Furthermore, since we are overestimating the average surface temperature and are neglecting heat losses from the channel to the environment, the h value is an upper limit. While this analysis is approximate, using the previously mentioned water properties and channel geometry as design criteria, it was estimated that the thermal development length for the devices was on the order of several centimeters, which was used for designing the devices for measurement of temperature profiles.

3.1.1. Experimental and simulation results

To experimentally measure the color transition length, defined as the distance at which the solution has just reached the temperature (33.3°C) corresponding to completion of its color transition, the PDMS-only devices along with the TuBeads mix were used as described in the Materials and Methods section. A representative image of the thermal profile observed in these experiments is shown in Figure 9. Notice that in the figure, for illustration purposes, the white ceramic surface of the hot plate used in the experiments was replaced with a metallic surface to make the color transition more evident. It can be noticed that the fluid completely changes color as it traverses the channel, it goes from a deep blue to a white color. From the flow rate measurements, it was determined that at maximum pressure the velocity inside the microchannels is smaller than 5 mm/s, which sets the maximum Reynolds number to ~ 10 . Then, for the pressure range used, inertia is not negligible in the Navier-Stokes Equations as discussed before.

Additional information can be obtained through the numerical simulation, shown in Figure 10. In Figure 10 (a), a cross section containing the mid-plane of the channels is shown. In the cross section we can observe that as liquid moves through the channel, its temperature increases till it is in thermal equilibrium with the surroundings. For the simulated pressures, color transition occurs within the first three turns, in agreement with what experimental observations. In Figure 10 (b), the surface temperature of the device is plotted; this temperature would correspond to what would be observed

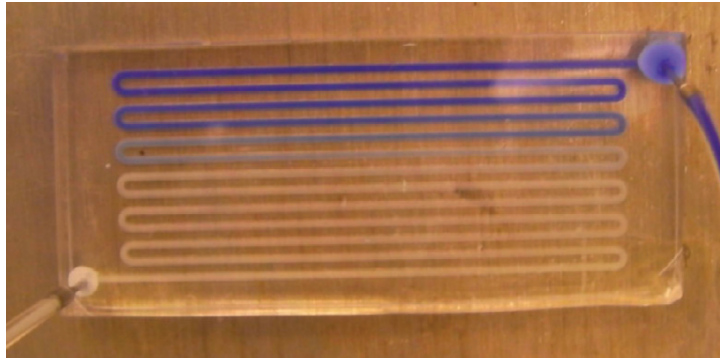


Figure 9. Color gradients observed using PDMS-only devices. In the figure, the color has fully transitioned at the 6th turn.

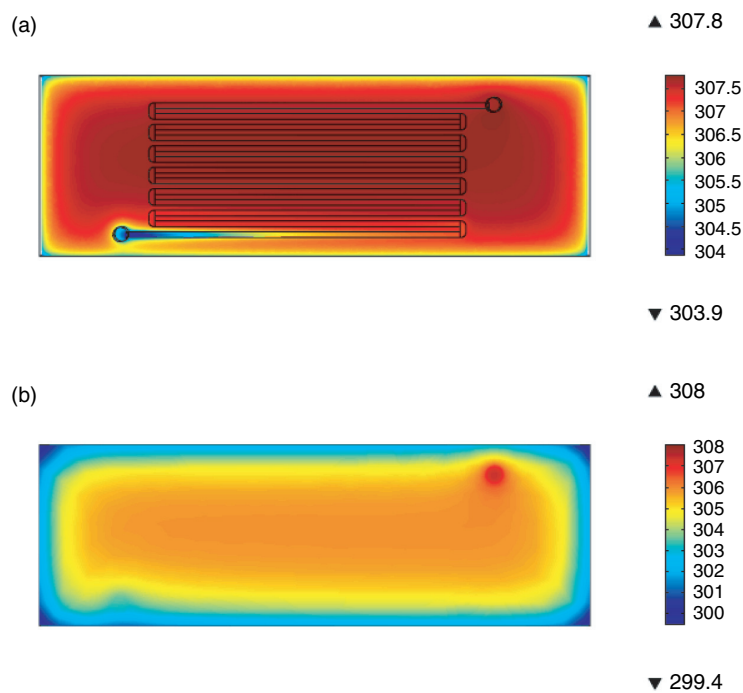


Figure 10. Representative Temperature Profiles obtained through simulation. (a) Temperature (in K) at the mid-plane cutting through the microfluidic channels, (b) Temperature distribution at the PDMS upper surface.

with an infrared camera. From the temperature distribution we can observe that at the surface almost all the details of the fluid thermal profile have been lost. There are indications of the fluid entering and leaving the domain, but it is difficult to determine the fluid temperature from the surface temperature profile.

In order to compare theory, experiment and simulation and gain a quantitative understanding of the method itself, the stream wise position (x) at which the fluid reached 33.3°C inside the channels was recorded and plotted in Figure 11 for different inlet pressures. This temperature was selected because it is the limit of the color change of the TuBeads mix, i.e. no further color change is observed after this

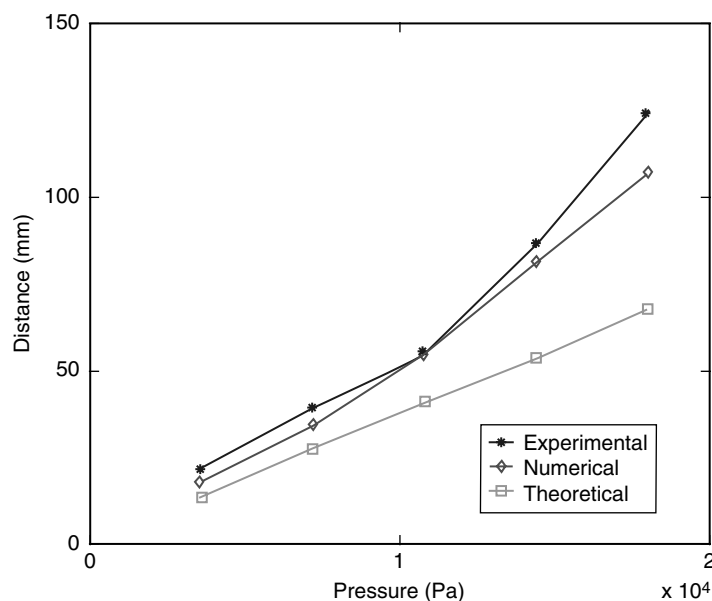


Figure 11. Effect of the device inlet pressure on the streamwise position in the microchannel at which the fluid has reached a temperature of 33.3°C.

temperature is reached, and provides an easier to read and compare signal. It must be noted that any other temperature within the sensitivity range can be selected if the imaging system is calibrated using the color sensitive chart described before in the Materials section.

First, we can notice that experimental and numerical values (simulated ones) show good agreement, the values and trends for the color transition length are similar, within 10% for the low pressure range and $\sim 20\%$ for the highest pressure used (18 kPa), which confirms the utility of the technique. The theoretical values under predict the color transition length as expected and discussed in the design section. Neglecting the heat loss through the upper surface of the device and assuming that the constant temperature plane surrounds the channel cause an overestimation of the heat transfer and an underestimation of the transition length. Further, the estimation of the wall temperature is by all means a crude approximation, which the numerical model was able to capture in a more accurate way.

Additionally, from the theoretical values, the main feature of the theoretical prediction can be observed: linear growth of the color transition length with pressure. Experimental and numerical values are not completely linear; the color transition length grows with pressure faster than linearly. This result suggest that the heat transfer coefficient is not a constant as assumed through the theoretical analysis, but a function of position, which can be the result of the sudden turns in the device and changes in the boundary conditions as fluid traverses the device, e.g. wall temperature as discussed before. Finally, as the pressure and flow rate increase, there is a larger uncertainty in the measurement of the thermal profile caused by the thermal iso-lines not being perpendicular to the flow direction, thus is not completely unexpected that at high pressures the measurement of isothermal positions have an increased inaccuracy.

3.2. TuBeads embedded devices

Finally, the ability to visualize temperature gradients inside the PDMS domain was verified using the TuBeads embedded devices. The experimental procedure was described in the materials and methods section. Figure 10 shows the color transition through the PDMS domain for an initial temperature of 4°C and an applied pressure of ~ 100 kPa. In Figure 12, undesired heat flow between different

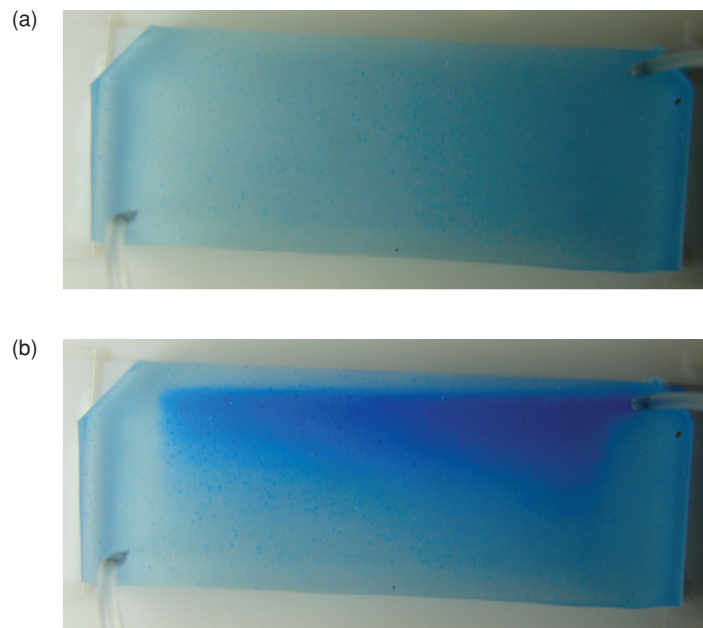


Figure 12. (a) TuBeads embedded device with bottom surface temperature set to 50°C. (b) TuBeads embedded PDMS thermal profile when cooled by water flowing from an inlet at 4°C at a driving pressure of ~100 kPa.

channels (thermal cross talking) can be easily distinguished; the color gradient profile is not only influenced by the streamwise distance from the inlet, but also by the distance from the inlet corner. The color gradient indicates heat flow through the PDMS within the channel's plane besides the dominant heat flow in the vertical direction, out of the channel's plane. Besides the thermal cross talking, we can also observe the effects of heat transfer in the PDMS material of the devices. Due to this heat transfer, thermal images obtained with the TuBeads embedded devices are not as sharp as those produced by flowing the TuBead mix, indicating that the temperature distribution in the PDMS material is different from that in the fluid. If the local wall temperature needs to be estimated it might be possible to coat the channel walls of the devices with beads, although a color transition over a small thickness might only be visible through a microscope.

4. CONCLUSIONS

As the number of miniaturized assays and devices that require temperature cycling increases, there is a need for techniques for thermal profile verification for the development of these devices. As microfluidic devices incorporate more complex and interdependent steps during assays, the verification of the correct local temperature conditions becomes critical during troubleshooting to isolate the possible failure modes. Furthermore, microfluidics can benefit from inexpensive and versatile methods capable of exploring thermal profiles locally, exactly where the reaction occurs.

In this manuscript we present an inexpensive, easy-to-use technique to measure local temperature profiles inside microchannels. Using encapsulated leuco dyes, temperatures between -5 to 60°C can be measured. Performance of the technique was evaluated by comparing the experimental color transition length as a function of applied pressure versus the values obtained through numerical simulation and a theoretical estimation. The thermal developing lengths obtained through this technique agree with the

numerical simulation.

Finally, the authors anticipate that this technique will be useful to the microfluidic community interested in developing inexpensive ways to measure, visualize and teach microfluidic heat transfer.

ACKNOWLEDGEMENTS

This work was supported in part by the Mexican National Science Foundation, CONACYT grant 205899 to MCA. The authors also acknowledge support from the Department of Mechanical Engineering and the Pappalardo II Laboratory at MIT. The authors wish to thank Professor Sang-Gook Kim for helpful discussions and Raymond Lam for support in conducting the experiments.

REFERENCES

- [1] P. Neuzil, C. Y. Zhang, J. Pipper, S. Oh, L. Zhuo, *Ultra fast miniaturized real-time PCR: 40 cycles in less than six minutes*, *Nucleic Acids Res.* 34(11) (2006) e77.
- [2] J. S. Marcus, W. F. Anderson, S. R. Quake, *Parallel picoliter RT-PCR assays using microfluidics*, *Anal. Chem.* 78 (3) (2006) 956–958.
- [3] K. Y. Lien, W. Y. Lin, Y. F. Lee, C. H. Wang, H. Y. Lei, and G. B. Lee, *Microfluidic systems integrated with a sample pretreatment device for fast nucleic-acid amplification*, *J. Microelectromech. Syst.* 17 (2) (2008) 288–301.
- [4] Z. Q. Niu, W. Y. Chen, S. Y. Shao, X. Y. Jia, W. P. Zhang, *DNA amplification on a PDMS-glass hybrid microchip*, *J. Micromech. Microeng.* 16 (2) (2006) 425–433.
- [5] D. S. Lee, S. H. Park, K. H. Chung, H. B. Pyo, *A disposable plastic-silicon micro PCR chip using flexible printed circuit board protocols and its application to genomic DNA amplification*, *IEEE Sens. J.* 8 (5–6) (2008) 558–564.
- [6] G. V. Kaigala, V. N. Hoang, A. Stickel, J. Lauzon, D. Manage, L. M. Pilarski, C. J. Backhouse, *An inexpensive and portable microchip-based platform for integrated RT-PCR and capillary electrophoresis*, *Analyst* 133 (3) (2008) 331–338.
- [7] D. S. Lee, S. H. Park, K. H. Chung, H. B. Pyo, *A disposable plastic-silicon micro PCR chip using flexible printed circuit board protocols and its application to genomic DNA amplification*, *IEEE Sens. J.* 8 (5–6) (2008) 558–564.
- [8] C. S. Zhang, D. Xing, Y. Y. Li, *Micropumps, microvalves, and micromixers within PCR microfluidic chips: Advances and trends*, *Biotechnol. Adv.* 25 (5) (2007) 483–514.
- [9] A. Jahn, W. N. Vreeland, M. Gaitan, L. E. Locascio, *Controlled vesicle self-assembly in microfluidic channels with hydrodynamic focusing*, *J. Am. Chem. Soc.* 126 (9) (2004) 2674–2675.
- [10] T. Thorsen, R. W. Roberts, F. H. Arnold, S. R. Quake, *Dynamic pattern formation in a vesicle-generating microfluidic device*, *Phys. Rev. Lett.* 86 (18) (2001) 4163–4166.
- [11] L. J. Kricka, P. Wilding, *Microchip PCR*, *Anal. Bioanal. Chem.* 377 (5) (2003) 820–825.
- [12] A. Pandey, M. Mann, *Proteomics to study genes and genomes*, *Nature* 405 (6788) (2000) 837–846.
- [13] Y. J. Kim, Y. K. Joshi, A. G. Fedorov, Y. J. Lee, S. K. Lim, *Thermal characterization of Interlayer Microfluidic Cooling of Three-Dimensional Integrated Circuits With Nonuniform Heat Flux*, *Journal of Heat Transfer* 132 (2010), 041009.
- [14] K. A. Cook-Chennault, N. Thambi and A. M. Sastry, *Powering MEMS portable devices – a review of non-regenerative power supply systems with special emphasis on piezoelectric energy harvesting systems*, *Smart Mat. and Struct.* 17, (2008), 043001.
- [15] C. Zhang, J. Xu, W. Ma., W. Zheng, *PCR Microfluidic devices for DNA amplification*, *Biotech. Adv.* 24, (2006) 243–284.
- [16] N. Crews, C. Wittwer, R. Palais and B. Gale, *Product differentiation during continuous-flow*

- thermal gradient PCR*, Lab On a Chip 8, (2008), 919–924.
- [17] C.Y. Lee, G.B. Lee, H.H. Liu, F.C. Huan, *MEMS-based Temperature Control Systems for DNA Amplification*, Int. J. Nonlinear Sci. and Num. Sim. 3, (2002) 215–218.
- [18] D. Ross, M. Gaitan, L. E. Locascio, *Temperature measurement in microfluidic systems using a temperature dependent fluorescent dye*, Anal. Chem. 73 (17) (2001) 4117–4123.
- [19] A. M. Chaudhari, T. M. Woundenberg, M. Albin, K. E. Goodson, *Transient liquid crystal thermometry of microfabricated PCR vessel arrays*, JMEMS 7 (4) (1998), 345–355.
- [20] R. Muthyala, *Chemistry and applications of leuco dyes*, Plenum Press (1997).
- [21] F. P. Incropera, D. P. DeWitt, T. L. Bergman, A. S. Lavine, *Introduction to Heat Transfer*, Wiley (2006).